# Thickness-tuned transition of band topology in $ZrTe_5$ nanosheets

Jianwei Lu,[1,2] Guolin Zheng,[1,2] Xiangde Zhu,[1] Wei Ning,[1,3,*] Hongwei Zhang,[1,2] Jiyong Yang,[1] Haifeng Du,[1,3] Kun Yang,[4] Haizhou Lu,[5] Yuheng Zhang,[1,2,3] and Mingliang Tian[1,2,3,*]

[1]*High Magnetic Field Laboratory, Chinese Academy of Sciences, Hefei 230031, Anhui, China*

[2]*Department of Physics, University of Science and Technology of China, Hefei 230026, China*

[3]*Collaborative Innovation Center of Advanced Microstructures, Nanjing University, Nanjing 210093, China*

[4]*National High Magnetic Field Laboratory, Florida State University, Tallahassee, Florida 32306-4005, USA*

[5]*Department of Physics, South University of Science and Technology of China, Shenzhen 518055, China*

(Received 8 November 2016; revised manuscript received 6 March 2017; published 29 March 2017)

We report thickness-tuned electrical transport in highly anisotropic three-dimensional Dirac semimetal $ZrTe_5$ nanosheets with thickness down to 10 nm. We find that the resistivity peak temperature $T^*$ can be significantly tuned by the nanosheet thickness. When the thickness is reduced from 160 to 40 nm, $T^*$ reduces systematically from 145 to 100 K. However, with the thickness further reducing to 10 nm, $T^*$ shifts up to a higher temperature. From our analysis, the system transitions from a topological semimetal with two types of carriers to a single band with conventional hole carriers when the thickness is less than 40 nm. Furthermore, by tracking the thickness dependence of the carrier density, we find that the Fermi level shifts continuously downward from the conduction band to the valence band with decreasing the thickness. Our experiment reveals a thickness-tuned transition of band topology in $ZrTe_5$ nanosheets which may be helpful for the understanding of the contrast observations in this material.

DOI: 10.1103/PhysRevB.95.125135

## I. INTRODUCTION

Zirconium pentatelluride ($ZrTe_5$), a fascinating new three-dimensional (3D) Dirac semimetal, has recently attracted considerable attention. It hosts rich quantum phenomena related to the chiral fermions in its highly anisotropic three-dimensional Dirac bands [1–3]. Comparing with other Dirac semimetals (e.g., $Cd_3As_2$ [4,5] and $Na_3Bi$ [6]), its electronic structure presents extreme sensitivity to external perturbations such as magnetic fields, temperature, elastic tension, or pressure [7–10]. For example, a recent angle-resolved photoemission spectroscopy (ARPES) experiment [11] shows that the temperature can induce a Lifshitz-type transition of electronic states from the hole band to electron band, leading to a resistance peak near the critical temperature $T^*$. The transport measurements on bulk $ZrTe_5$ also have demonstrated clear changes from hole-dominated states above $T^*$ to electron-dominated states below $T^*$ [9,12]. While the gapless topological Dirac semimetal phase has been confirmed in bulk $ZrTe_5$ [1,2,13–15], recent scanning-tunneling microscopy experiments surprisingly detected a bulk band gap with topological edge states at the surface step edge, which indicated that single-layered $ZrTe_5$ might be a two-dimensional topological insulator that could host the quantum spin-Hall effect [16–18]. These contrasting results indicate that the thickness, as an alternative way, may effectively tune the electronic structure in $ZrTe_5$, although so far the mechanism has not been fully explored.

In this paper, we study the transport properties of $ZrTe_5$ nanosheets with thickness down to 10 nm. We find that the resistivity anomaly temperature $T^*$ systematically shifts toward lower temperatures as the thickness reduces to 40 nm, indicating the suppression of the electron carriers in the Dirac band. When the nanosheet thickness is less than 40 nm, a broad resistive peak shows up at higher temperatures which moves up to room temperature with thickness further reduced to 10 nm. Both longitudinal resistivity and Hall resistivity measurements demonstrate that the resistance peak in thinner nanosheets (<40 nm) has a different origin from the bulk, where carriers in a secondary hole band dominate the transport. By tracking the carrier densities, a consecutive downward shifting of the Fermi level from conduction band to valence band is demonstrated to decrease the thickness down to 10 nm, which reveals a thickness-tuned transition of the band topology in $ZrTe_5$ nanosheets.

## II. EXPERIMENTAL TECHNIQUES

$ZrTe_5$ single crystals were grown via the iodine vapor transport method in a two-zone furnace as described in Ref. [19]. Stoichiometric amounts of elements Zr (99.99%) and Te (99.99%) lumps with 5 mg/cm$^3$ iodine were sealed in an evacuated quartz tube. The quartz tube was heated and kept at 590 °C for 2 days. Then the furnace gradient was kept between 590 and 380 °C for 14 days before turning off the furnace. To obtain high-quantity $ZrTe_5$ crystals, the high purity and nonoxidation of Te lumps is important. The obtained crystals show a thin, elongated rectangular shape with length up to centimeters. In this work, all the nanosheets were mechanically exfoliated from the bulk crystals, followed by directly transferring onto $Si/SiO_2$ substrate. Hall-bar devices were fabricated by standard electron-beam lithography followed by a Au (80 nm)/Ti (10 nm) evaporation and lift-off process. Transport measurements were performed with a physical properties measurement system.

## III. RESULTS AND DISCUSSION

Figure 1(a) shows the normalized temperature dependence of resistance of $ZrTe_5$ nanosheets with different thicknesses.

*Author to whom correspondence should be addressed: ningwei@hmfl.ac.cn; tianml@hmfl.ac.cn

 

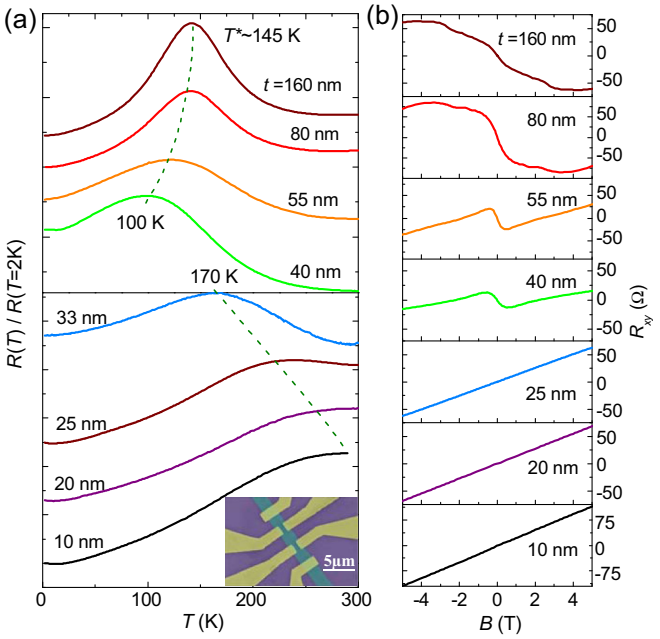


FIG. 1. (a) Normalized temperature dependence of longitudinal resistance $ZrTe_5$ nanosheets with different thicknesses. All curves are offset vertically for clarity. Inset: SEM image of a Hall-bar device used in the measurement. (b) Hall resistivity of the nanosheets with different thicknesses measured at $T = 2$ K.

In the thick samples (e.g., $t = 160$ nm), the resistivity peak temperature $T^*$, defined from the peak position of the resistance-temperature ($R_{xx} - T$) curve, is about 145 K, which is consistent with the value in bulk single crystals [12,20]. As the thickness is reduced to 40 nm, $T^*$ decreases systematically to about 100 K. Strikingly, when the thickness is reduced to 33 nm, a broad peak appears near 170 K which further shifts up to 300 K for the $t = 20$ nm sample. Figure 1(b) shows the Hall resistivity $R_{xy}$ of these nanosheets measured at 2 K. For sample $t = 160$ nm, $R_{xy}$ exhibits a typical multiband property with the electron band dominating the transport. With decreasing the thickness to 80 nm, the Hall coefficient $R_H \propto R_{xy}/B$, with $B$ the magnetic field, shows a sign reversal from negative in the low-field range to positive near 4 T. Such a reversal is more pronounced for samples $t = 55$ and 40 nm. As a comparison, for samples $t = 25$, 20, and 10 nm, $R_{xy}$ shows a linear field dependence. This result indicates that the electron band is suppressed with the thickness decrease and the hole carriers take over the transport properties in thin samples ($t < 40$ nm). Hence, the role of decreasing thickness has the same effect of lifting up temperature, i.e., lowering the Fermi level or shifting up the hole band. However, we note that the nanosheets with $t < 40$ nm present a metallic behavior, which is in contrast to the semiconductive hole band above $T^*$ in thick samples. In other words, the hole carriers of the nanosheets $t < 40$ nm are probably not from the same hole band as indicated at high temperatures.

The long-standing question of the mechanism for the resistance peak at $T^*$ is currently attributed to the upward shift of the Fermi level from the Dirac hole band to electron band with decreasing temperature [21], i.e., the temperature-induced Lifshitz transition [11]. This can also be verified by the temperature-dependent Hall-resistivity measurement for our thick nanosheets, e.g., $t = 55$ nm, as shown in Fig. 2(a), where the Hall coefficient $R_H$ near zero field shows a sign reversal from positive to negative near the peak temperature $T^*$ (~120 K). To explore the electronic mechanism of the resistance anomaly in thin nanosheets ($t < 40$ nm), we have measured the Hall resistivity at different temperatures of sample $t = 33$ nm. As shown in Fig. 2(b), the Hall resistivity shows a linear behavior with a positive slope, regardless of the temperature being below or above $T^*$ (~170 K), which provides evidence that the hole carrier band dominates the transport in thinner nanosheets ($t < 40$ nm), and no transition of band topology occurs with temperature cooling through $T^*$. In other words, the origin of the broad resistance peak in thinner nanosheets cannot be attributed to the competition between electron and hole pockets, which is different from the thick samples ($t > 40$ nm).

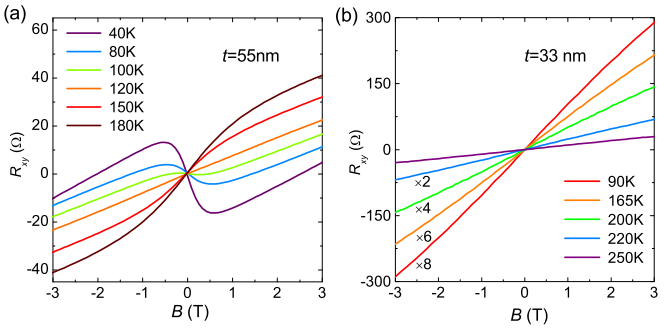


FIG. 2. Hall resistivity under different temperatures near $T^*$ in $ZrTe_5$ nanosheets with thickness (a) $t = 50$ nm and (b) $t = 33$ nm.

To have a comprehensive insight on this conventional resistivity anomaly in thinner samples, we have tracked the temperature dependence of carrier density and mobility in samples $t = 33$ and 25 nm, as shown in Fig. 3. Since the Hall resistivity of both samples exhibits a linear behavior, we can evaluate the carrier density by the formula $n = 1/R_H e$, and the mobility $\mu$ by the relationship $\mu = \sigma/ne$, where $e$, $\sigma$, and $n$ are the electron charge, zero-field conductivity, and carrier density, respectively. For both samples, the carrier

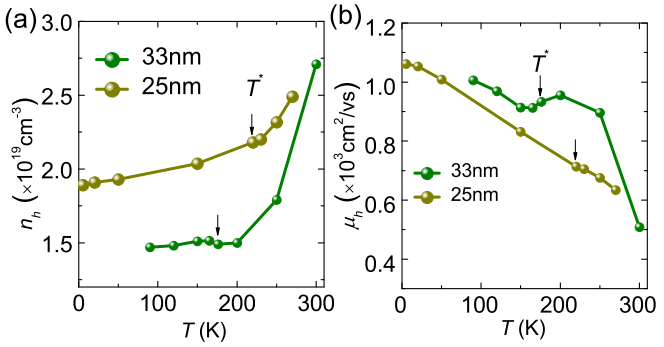


FIG. 3. Temperature dependence of the carrier density (a) and mobility (b) in $t = 33-$ and 25-nm-thick samples. $T^*$ is the resistivity anomaly temperature for different samples.

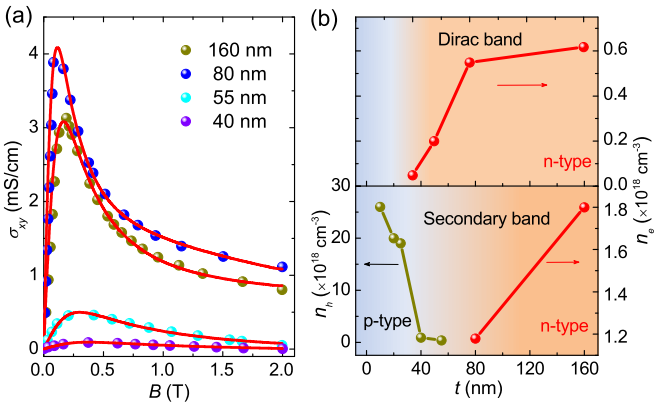


FIG. 4. (a) Two-band fitted Hall conductivity for nanosheets with thickness above 40 nm. The red curves are the fitting results while the solid circles are the experimental data. (b) The evolution of the carrier density as function of the thickness. $n_e$ and $n_h$ denote the electron and hole carrier density, respectively. Above 40 nm, the band structure consists of two electron pockets: a 3D Dirac band (with low carrier density and high mobility) and a secondary band. Below 40 nm, only a single hole band is revealed.

density decreases sharply with temperature decrease while the mobility shows an opposite trend and increases gradually. Thus the broad resistivity peak is likely formed due to the opposite contributions of reducing charge-carrier density $n$ and increasing mobility $\mu$ to the electrical resistivity. We note that similar upward shifting of the resistance anomaly temperature $T^*$ has been observed in several works on $ZrTe_5$ nanosheets [22,23].

To fully understand the thickness-tuned band topology, we have tracked the thickness dependence of carrier density at $T = 2$ K. As shown in Fig. 4, for nanosheets with $t \geqslant 40$ nm, the two-band model was used to fit the Hall conductivity $\sigma_{xy}$,

$$\sigma_{xy}(2\text{ K}) = \left[ n_1\mu_1^2 \frac{1}{1+(\mu_1 B)^2} + n_2\mu_2^2 \frac{1}{1+(\mu_2 B)^2} \right] eB, \tag{1}$$

where $n_1$ and $n_2$ are the carrier density in two different bands, and $\mu_1$ and $\mu_2$ are the mobility, correspondingly. Figure 4(a) shows the fitting result of Hall conductivity for samples $t \geqslant 40$ nm. The extracted carrier density as the function of thickness is shown in Fig. 4(b). In thick nanosheets $t > 80$ nm, it contains a Dirac electron pocket with high mobility and a secondary electron band with low mobility. This result is consistent with recent ARPES experiments, where an off-centered secondary band is revealed, beside the Dirac band at the Brillouin zone center [1,3,11]. The carrier densities in both electron pockets decrease with reducing thickness, hinting at a downward shifting of the Fermi level. In samples $80\text{ nm} \leqslant t \leqslant 40$ nm, the carriers in the secondary band transform from $n$- to $p$ type, while in samples below 40 nm, only a single band with $p$-type carriers is revealed due to the linear behavior of Hall resistivity (shown in Figs. 2 and 3). This $p$-type carrier density increases while decreasing the thickness down to 10 nm [shown in Fig. 4(b)]. These results demonstrate that from $t = 160$ to 10 nm, the Fermi level shifts consecutively from the conduction band down to the valence band, which reveals a thickness-tuned band topology transition in $ZrTe_5$ nanosheets.

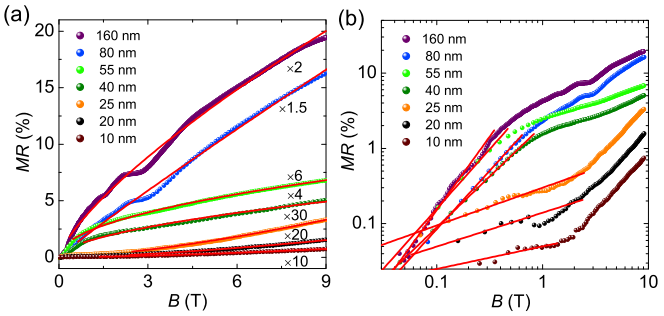


FIG. 5. (a) MR curves of $ZrTe_5$ nanosheets with different thicknesses measured at $T = 2$ K. (b) The log-log plot of the MR curves. The red curves are the fitting curves with a formula of $R \propto B^{\alpha}$.

To gain deeper understanding of the electronic nature of $ZrTe_5$ nanosheets, we have explored the longitudinal magnetoresistance (MR) of samples with different thicknesses, as shown in Fig. 5. When fitting the MR curve by a formula of $R \propto B^{\alpha}$, with $\alpha$ the fitting parameter, it is clear that the MR presents a quasilinear behavior with an exponent $\alpha$ close to 1 in thick nanosheets ($(t \geqslant 80\text{ nm})$). Such a linear MR has been widely seen in topological insulators and topological semimetals with linear energy dispersion [24–26]. For samples $t = 55$ and 40 nm, the MR follows a $\sqrt{B}$-type behavior with $\alpha \sim 0.5$, indicating the weak antilocalization (WAL) effect in a 3D topological semimetal [27]. In contrast, the MR exhibits a simple quasiquadratic behavior with $\alpha \sim 1.6$ when the thickness is less than 40 nm. When tracking the MR behavior in a very low-field region, we found that the MR exhibits a quasiquadratic behavior with $\alpha \sim 2$ for thick nanosheets ($t \geqslant 40$ nm), as shown in the log-log plot of the MR curves in Fig. 5(b), while for nanosheets $t < 40$ nm, the low-field MR shows a $\sqrt{B}$ tendency with $\alpha \sim 0.5$. As discussed above, the Fermi level shifts downward consecutively to the Dirac point with decreasing thickness. Thus, it can be inferred that the $\sqrt{B}$-type MR induced by the WAL effect in the presence of the weak intervalley scattering will surpass the $B^2$-type MR when decreasing the thickness below 40 nm. Unfortunately, we cannot determine whether or not there is a band gap in the Dirac band in the thinner nanosheets since no Shubnikov–de Haas (SdH) quantum oscillations were observed in our studied field range. The fact that the nanosheets with $t < 40$ nm show excellent metallic behavior with hole carriers demonstrates that the secondary hole bands dominate the transport and most likely have a conventional nature. This is qualitatively consistent with recent magnetoinfrared spectroscopy experiments in thin $ZrTe_5$ nanoflakes, where a zero magnetic field optical absorption with a photon energy of 10 meV hints at the existence of 3D massive Dirac fermions for thin $ZrTe_5$ nanosheets [28].

## IV. CONCLUSION

In conclusion, we have systematically studied the transport properties of 3D Dirac semimetal $ZrTe_5$ nanosheets with different thicknesses. We found that the resistivity anomaly

temperature evolves nonmonotonically with decreasing the thickness. Detailed Hall measurements suggest that the anomalous resistivity with the peak in thinner $ZrTe_5$ nanosheets ($t < 40$ nm) stems from a totally different mechanism from that in thick samples (($t \geqslant 40$ nm)). Further analysis of the carrier density demonstrates that the Fermi level shifts consecutively from conduction band to valence band with decreasing thickness. Our experiments provide a comprehensive insight into the thickness-dependent electronic structures in 3D Dirac semimetal $ZrTe_5$, which would be helpful for the understanding of this complex layered material and further study on nanodevices.

## ACKNOWLEDGMENTS

This work was supported by the Natural Science Foundation of China (Grants No. 11574320, No. 11174294, No. 11374302, No. 11204312, No. 11474289, and No. U1432251), and the National Key Research and Development Program of China (Grant No. 2016YFA0401003), the program of Users with Excellence, the Hefei Science Center of CAS, the CAS/SAFEA international partnership program for creative research teams of China, and National Science Foundation through Grants No. DMR-1004545 and No. DMR-1442366.

J.L. and G.Z. contributed equally to this work.

[1] Q. Li, D. E. Kharzeev, C. Zhang, Y. Huang, I. Pletikosić, A. V. Fedorov, R. D. Zhong, J. A. Schneeloch, G. D. Gu, and T. Valla, Nat. Phys. **12**, 550 (2016).

[2] G. Zheng, J. Lu, X. Zhu, W. Ning, Y. Han, H. Zhang, J. Zhang, C. Xi, J. Yang, H. Du, K. Yang, Y. Zhang, and M. Tian, Phys. Rev. B **93**, 115414 (2016).

[3] L. Shen, M. X. Wang, S. C. Sun, J. Jiang, X. Xu, T. Zhang, Q. H. Zhang, Y. Y. Lv, S. H. Yao, Y. B. Chen, M. H. Lu, Y. F. Chen, C. Felser, B. H. Yan, Z. K. Liu, L. X. Yang, and Y. L. Chen, J. Electron. Spectrosc. Relat. Phenom. (2016), doi:10.1016/j.elspec.2016.10.007.

[4] Z. K. Liu, J. Jiang, B. Zhou, Z. J. Wang, Y. Zhang, H. M. Weng, D. Prabhakaran, S.-K. Mo, H. Peng, P. Dudin, T. Kim, M. Hoesch, Z. Fang, X. Dai, Z. X. Shen, D. L. Feng, Z. Hussain, and Y. L. Chen, Nat. Mater. **13**, 677 (2014).

[5] M. Neupane, S.-Y. Xu, R. Sankar, N. Alidoust, G. Bian, C. Liu, I. Belopolski, T.-R. Chang, H.-T. Jeng, H. Lin, A. Bansil, F. Chou, and M. Z. Hasan, Nat. Commun. **5**, 3786 (2014).

[6] Z. K. Liu, B. Zhou, Y. Zhang, Z. J. Wang, H. M. Weng, D. Prabhakaran, S.-K. Mo, Z. X. Shen, Z. Fang, X. Dai, Z. Hussain, and Y. L.Chen, Science **343**, 864 (2014).

[7] E. P. Stillwell, A. C. Ehrlich, G. N. Kamm, and D. J. Gillespie, Phys. Rev. B **39**, 1626 (1989).

[8] Y. H. Zhou, J. F. Wu, W. Ning, N. Li, Y. P. Du, X. L. Chen, R. R. Zhang, Z. H. Chi, X. F. Wang, X. D. Zhu, P. C. Lu, C. Ji, X. G. Wan, Z. R. Yang, J. Sun, W. G. Yang, M. L. Tian, Y. H. Zhang, and H.-K. Mao, Proc. Natl. Acad. Sci. USA **113**, 2904 (2016).

[9] Y. W. Liu, X. Yuan, C. Zhang, Z. Jin, A. Narayan, C. Luo, Z. G. Chen, L. Yang, J. Zou, X. Wu, S. Sanvito, Z. C. Xia, L. Li, Z. Wang, and F. Xiu, Nat. Commun. **7**, 12516 (2016).

[10] G. Zheng, X. Zhu, J. Lu, W. Ning, H. Zhang, W. Gao, Y. Han, J. Yang, H. Du, K. Yang, Y. Zhang, and M. Tian, arXiv:1607.05384.

[11] Y. Zhang, C. Wang, L. Yu, G. Liu, A. Liang, J. Huang, S. Nie, Y. Zhang, B. Shen, J. Liu *et al.*, arXiv:1602.03576.

[12] D. N. McIlroy, S. Moore, D. Q. Zhang, J. Wharton, B. Kempton, R. Littleton, M. Wilson, T. M. Tritt, and C. G. Olson, J. Phys.: Condens. Matter. **16**, L359 (2004).

[13] G. Manzoni, A. Crepaldi, G. Autès, A. Sterz, F. Cilento, A. Akrap, I. Vobornik, L. Gragnaniello, Ph. Bugnon, M. Fonin, H. Berger, M. Zacchigna, O.V. Yazyev, and F. Parmigiani, J. Electron. Spectrosc. Relat. Phenom. (2016), doi:10.1016/j.elspec.2016.09.006.

[14] R. Y. Chen, Z. G. Chen, X.-Y. Song, J. A. Schneeloch, G. D. Gu, F. Wang, and N. L. Wang, Phys. Rev. Lett. **115**, 176404 (2015).

[15] R. Y. Chen, S. J. Zhang, J. A. Schneeloch, C. Zhang, Q. Li, G. D. Gu, and N. L. Wang, Phys. Rev. B **92**, 075107 (2015).

[16] H. Weng, X. Dai, and Z. Fang, Phys. Rev. X **4**, 011002 (2014).

[17] R. Wu, J. Z. Ma, S. M. Nie, L. X. Zhao, X. Huang, J. X. Yin, B. B. Fu, P. Richard, G. F. Chen, Z. Fang, X. Dai, H. M. Weng, T. Qian, H. Ding, and S. H. Pan, Phys. Rev. X **6**, 021017 (2016).

[18] X. B. Li, W. K. Huang, Y. Y. Lv, K. W. Zhang, C. L. Yang, B. B. Zhang, Y. B. Chen, S. H. Yao, J. Zhou, M. H. Lu, L. Sheng, S. C. Li, J. F. Jia, Q. K. Xue, Y. F. Chen, and D. Y. Xing, Phys. Rev. Lett. **116**, 176803 (2016).

[19] G. N. Kamm, D. J. Gillespie, A. C. Ehrlich, T. J. Wieting, and F. Levy, Phys. Rev. B **31**, 7617 (1985).

[20] T. M. Tritt, N. D. Lowhorn, R. T. Littleton, A. Pope, C. R. Feger, and J. W. Kolis, Phys. Rev. B **60**, 7816 (1999).

[21] G. Manzoni, A. Sterzi, A. Crepaldi, M. Diego, F. Cilento, M. Zacchigna, P. Bugnon, H. Berger, A. Magrez, M. Grioni, and F. Parmigiani, Phys. Rev. Lett. **115**, 207402 (2015).

[22] J. Niu, J. Wang, Z. He, C. Zhang, X. Li, T. Cai, X. Ma, S. Jia, D. Yu, and X. Wu, Phys. Rev. B. **95**, 035420 (2017).

[23] G. Qiu, Y. Du, A. Charnas, H. Zhou, S. Jin, Z. Luo, D. Y. Zemlyanov, X. Xu, G. J. Cheng, and P. D.Ye, Nano Lett. **16**, 7364 (2016).

[24] A. Narayanan, M. D. Watson, S. F. Blake, N. Bruyant, L. Drigo, Y. L. Chen, D. Prabhakaran, B. Yan, C. Felser, T. Kong, P. C. Canfield, and A. I. Coldea, Phys. Rev. Lett. **114**, 117201 (2015).

[25] X. Wang, Y. Du, S. Dou, and C. Zhang, Phys. Rev. Lett. **108**, 266806 (2012).

[26] J. Feng, Y. Pang, D. Wu, Z. Wang, H. Weng, J. Li, X. Dai, Z. Fang, Y. Shi, and L. Lu, Phys. Rev. B **92**, 081306(R) (2015).

[27] H. Lu and S.-Q. Shen, Phys. Rev. B **92**, 035203 (2015).

[28] Z. G. Chen, R. Y. Chen, R. D. Zhong, J. Schneeloch, C. Zhang, Y. Huang, F. M. Qu, R. Yu, Q. Li, G. D. Gu, and N. L. Wang, Proc. Natl. Acad. Sci. USA **114**, 816 (2017).